

Original Article

Characterization of Acceleration Shock Pulse by Finite Element Analysis and Validation by Shock Testing on Heavy Mass Test Objects for Defense Applications

Dattatraya R Hipparkar^{1*}, Mukesh Singh Baghel¹, Sunil Chandel¹

¹Defence Institute of Advanced Technology, Pune, India

^{1*}Corresponding Author : dhipparkar@rediffmail.com

Received: 14 March 2023

Revised: 06 May 2023

Accepted: 23 May 2023

Published: 25 June 2023

Abstract - Shock Testing is an essential evaluation criterion to assess the performance of newly designed systems for their dynamic performance. There are various methods to generate a shock pulse for shock testing, like free fall drop test, horizontal impact, kick, and explosion. The primary purpose of this research is to design and characterize the pulse shaper of neoprene rubber for Shock testing of heavy objects. This paper presents an implicit Finite-Element (FE) model of the impact of a test table on a rubber disc. The FE model is used to study the influence of drop height, the mass of the object, and the thickness of the pulse shaper on shock pulse characteristics. Shock tests were also conducted on the test stand, and a comparison of the results from the FE and experimental data is presented in this paper.

Keywords - Drop test, FEM analysis, Hyperelastic, Neoprene rubber shock pulse.

1. Introduction

Ground tests are the most critical task in approving new engineering, scientific, and technological solutions. They also detect possible design and technical errors made in designing and manufacturing. Shock tests are essential to experimental ground tests of products since the theoretical derivation of shock-related phenomena is tedious, cumbersome, and nonlinear. The shock pulse shape, amplitude, and duration are controlled as a function of the test table and the object's total weight, impact speed, and various pulse-shaping materials placed on the impact surfaces [1].

There is a paramount concern for devices with high acceleration applications, such as missile control systems. The acceleration pulse shape is critical to high acceleration shock testing as clean, consistent pulse shapes are highly complicated to obtain [2]. High acceleration shock test methods include Hopkinson pressure bar (HPB) techniques [4, 5].

A structure should resist shock, i.e. bear shock loads without destruction and function normally under environmental shock loads. Shock stability and shock resistance cannot be verified in full scope by a design method and are certified only in the case of their tests on shock stands.

A component or system should resist shock and function generally under environmental shock loads. However, a

design method cannot verify shock stability and resistance in totality and is certified only in the case of their tests on shock stands.

A Shock testing stand is a mechanical device that applies a mechanical shock to equipment under test. The test item is placed on a table that impacts a pulse shaper material in the horizontal impact method. This impact generates a shock pulse on the test object. The following three parameters define the shock pulse's shape, including its amplitude and time duration.

- Mass of the object
- Stiffness of pulse shaper
- Drop Height

There is various material used as pulse shaper to generate a shock pulse. For a half sinusoidal pulse, generally, elastomers are used as a pulse shaper material [7]. In this study, a Neoprene rubber is taken as pulse shaper material, and its properties have been established for FEM simulation. FEM simulation is carried out for a different combination of object masses, pulse shaper stiffness, and drop heights. Shock tests were also conducted on pendulum-type horizontal shock testing machines to validate the FEM model.

There are very few shock test machines available around the globe, and they have limited capacity. This paper presents the characterization of acceleration pulse on a shock test



machine for neoprene rubber. The Comparative study of the influence of varying mass, drop height, and pulse shaper thickness on pulse shape is done for the neoprene rubber material.

The literature on the neoprene rubber material is unavailable, and the author has studied this in this paper. The selection of pulse shaper material is the most important task for shock pulse generation. The pulse's shape and magnitude depend on the shaper material properties. Usually, elastomers are used to generate a half-sign pulse. There are various elastomers, i.e., Natural Rubber, Nitrile Butadiene Rubber, Neoprene Rubber, etc., are available for pulse shaper material; Neoprene material is selected by comparing different properties for the pulse shaper like rebound and tear resistance.

2. Mechanical Properties of Pulse Shaper

There are several methods to generate a half-sine pulse. However, using elastomer as a pulse shaper is the most widely used technique. This is because the elastomer's mechanical properties define the shock pulse's amplitude and time duration. For this study, a rubber disc made of a special Neoprene compound has been developed for heavy-weight impact. During the impact, the disc is only subjected to compression. Hence, the mechanical properties in static compression have been established in accordance with ASTM D 575 [8] for three specimens. The test specimen size was $\varnothing 28.5 \text{ mm} \times 15 \text{ mm}$, as shown in Fig. 1.



Fig. 1 Test Specimen for Compression Test

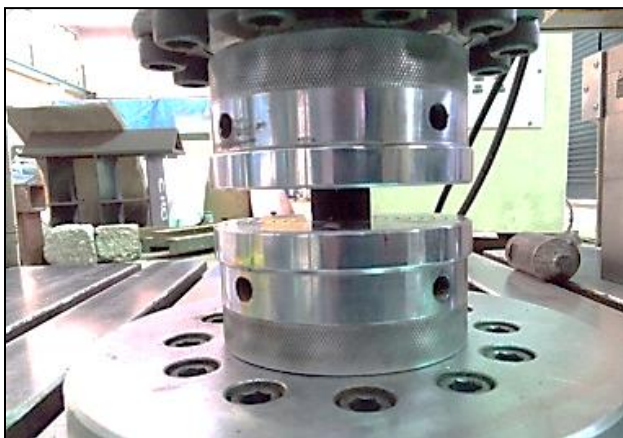


Fig. 2 Test Set up for Compression test

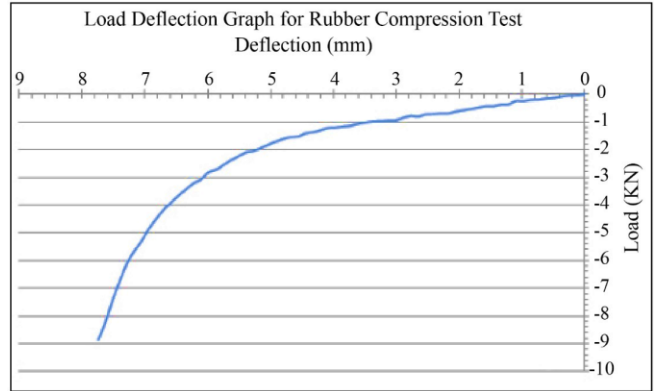


Fig. 3 Loads vs. Deflection graph

Force was applied with a deflection rate of 12 mm/min. Force was measured for each step of 0.5 mm up to 8.5 mm deflection. The average force vs. deflection result is shown in Fig. 3. Fig. 3 depicts that the initial stiffness until 5 mm deflection is linear, post which the deflections become nonlinear.

3. FEM Simulation

This study aims to compare and correlate the FEA results of acceleration response on the test object with experimental results during the shock test and then analyze the effect of different variables on the shock pulse shape. A numerical model is developed to analyze the acceleration response on test objects during impact on the pulse shaper. A schematic diagram of the Horizontal Shock Testing Machine (STM) is shown in Fig 4.

In this study, pulse shaper(s) is fixed with a suspended structure called buffer mass, and the test object is rigidly connected with the striker. The test object is released from a predetermined height and impacts the pulse shaper, resulting in a shock pulse on the test object.

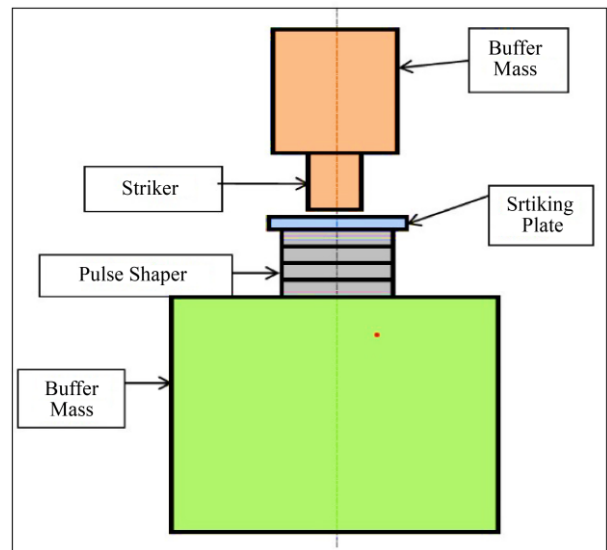


Fig. 4 (a) Schematic diagram 2D representation of the problem

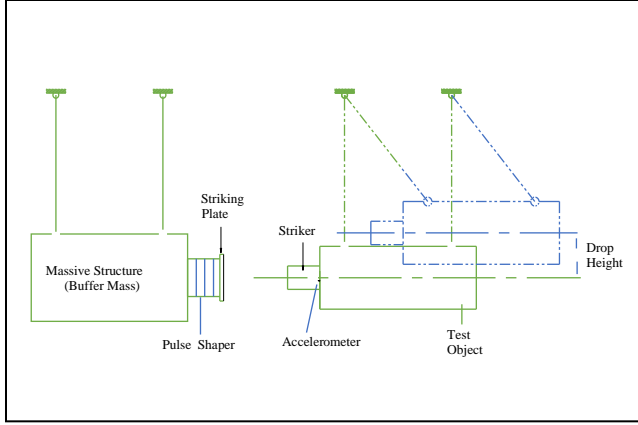


Fig. 4(b) Schematic diagram of Horizontal Shock Testing Machine

In the present analysis, the impact is simulated as an axisymmetric problem using the implicit method. The implicit method provides a high level of accuracy as compared to the explicit approach. Finite element (FE) code ABAQUS 6.12-1 has been used for impact simulation.

Since the loading and geometry of the test object are symmetrical about the axis, the impact is simulated as an axisymmetric model. Therefore, it is considered that the test object is rigidly connected to the striker, and both parts are modeled as integral parts of the test bed.

In the present simulation, the size of each shaper was $\text{Ø}520 \text{ mm} \times \text{Ø}180 \text{ mm} \times 50 \text{ mm}$. Simulations were carried out for three pulse shaper thicknesses: 200 mm, 300 mm, and 400 mm. The required pulse shaper thickness was achieved by using multiple shapers. Similarly, the length of the test object was calculated to get the required mass value.

The next step after the geometrical model is a material model. This step assigns material properties to each part of the assembled structure. There are a total of five elements in the assembly. All the elements, except the pulse shaper, have been modeled using Young's modulus 200GPa, Poisson's ratio 0.3, and density 7850 kg/m³.

Table 1. Geometrical parameters for the model

Sr. No.	Part Name	Parameter	Values (m)
1	Buffer Mass	Diameter	Ø2.3
		Length	1.5
2	Striker	Diameter	Ø0.2
		Length	0.26
3	Striking Plate	Diameter	Ø0.6
		Thickness	0.05
4	Pulse Shaper	Outer Diameter	Ø0.52
		Inner Diameter	Ø0.18
		Thickness	0.05
5	Test Object	Diameter	Ø0.2

Table 2. Element types used for the model

Sr. No.	Part	Element Types
1	Buffer Mass	CAX4R
2	Striker	CAX4R
3	Striking Plate	CAX4R
4	Pulse Shaper	CAX4RH
5	Test Object	CAX4R

Since the pulse shaper is rubber, it is modeled as Hyperelastic material. A hyper-elastic material model derives its stress-strain relationship from a strain-energy density function. Therefore, a suitable strain energy function is required to model the hyper-elastic material. The "best" strain energy function is the one that best matches the experimental data over the stretch range of interest. The test data has been evaluated with different energy functions to define the strain energy function, and the Yeoh model was the best-suited strain energy model.

A mesh convergence study was carried out for the model. The mesh convergence was carried out with an element size of 1mm. Element type and no. of elements associated with different parts of the model are given in Table 2.

The simulation was done using Implicit FE code, and impact velocity was given to test the object as an initial condition. Different impact velocities have been used for each mass and each pulse shaper thickness. Impact velocity is calculated for different drop heights as 100 mm, 200mm, 300 mm, 400 mm, 500 mm, 600 mm, and 700 mm for simulation.

Acceleration amplitude, time period, and maximum strain in the pulse shaper were recorded. The result data of acceleration contains some numerical noise, as shown in Fig. 5.

Fast Fourier Transform (FFT) was done to find out the numerical noise content of the data. FFT of the same data is shown in Fig. 6.

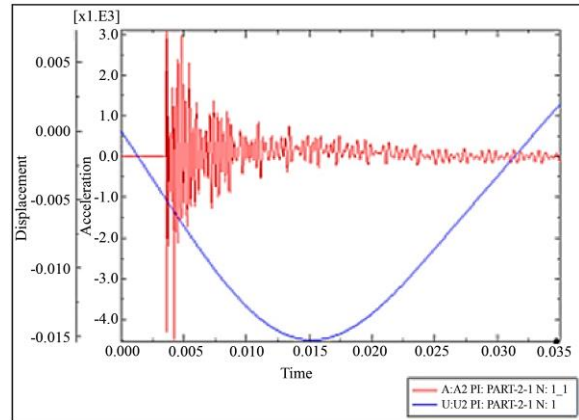


Fig. 5 Unfiltered acceleration and displacement data

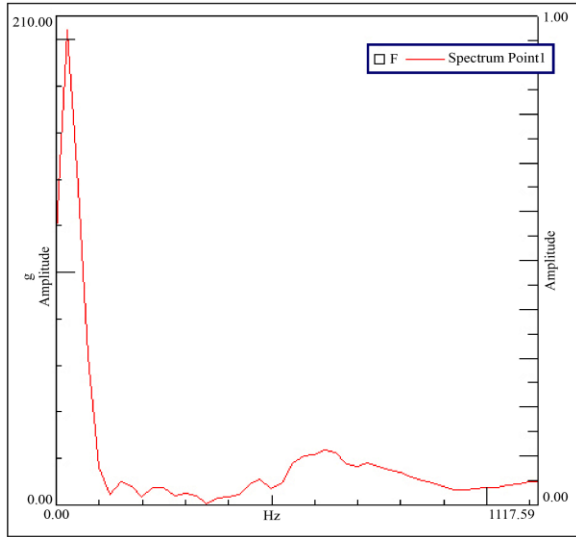


Fig. 6 FFT of unfiltered acceleration data

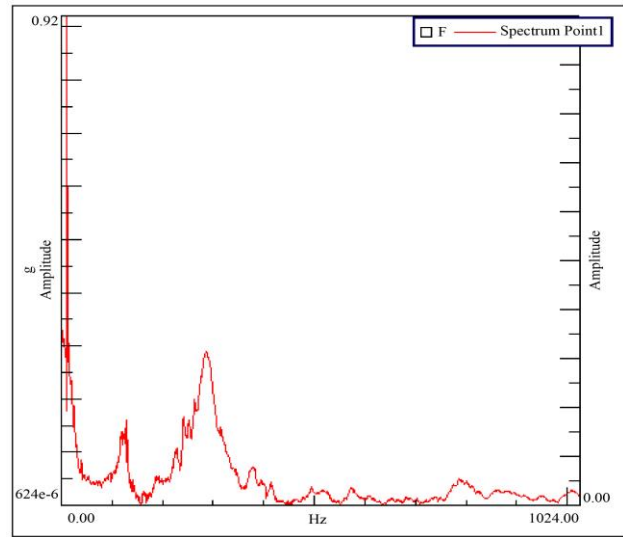


Fig. 9 FFT of original acceleration data

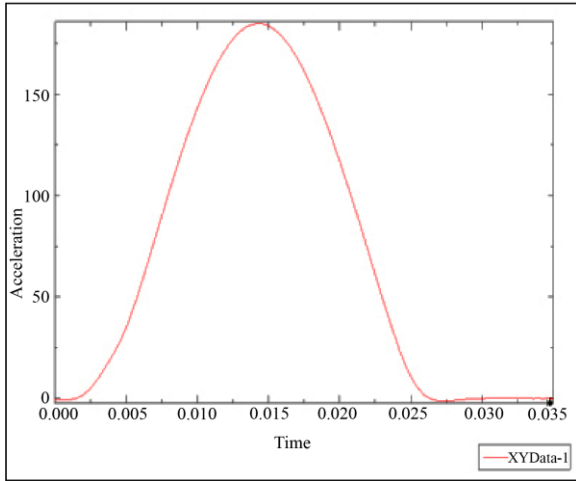


Fig. 7 Filtered acceleration data

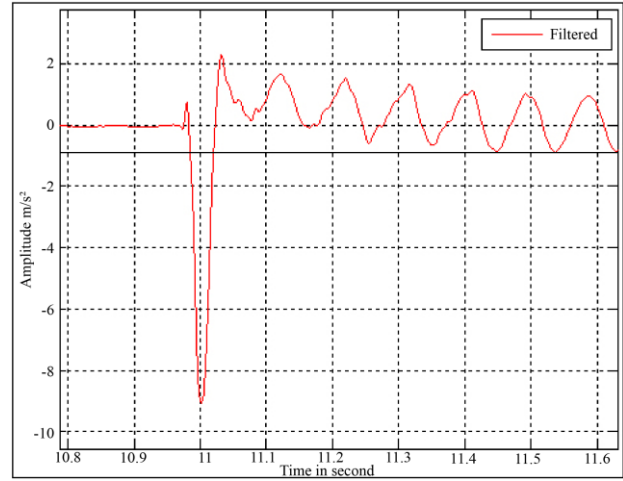


Fig. 10 Filtered acceleration-time data

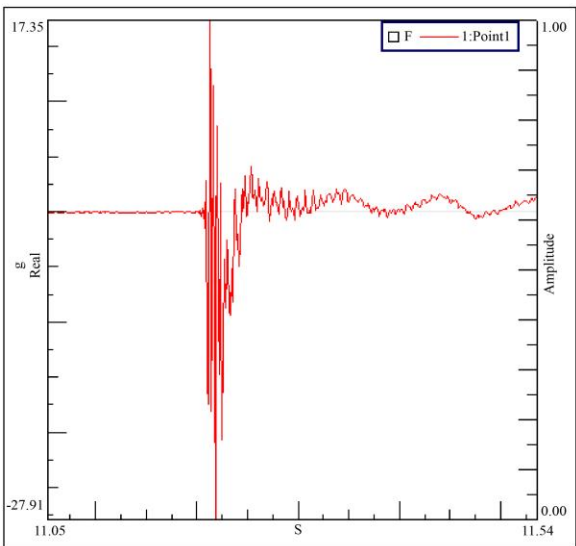


Fig. 8 Acquired acceleration-time data

After FFT analysis, it was found that frequencies above 150 Hz could be filtered out. So, the unfiltered data was filtered with a low pass filter with a cut-off frequency of 150 Hz. A filtered acceleration data is shown in Fig.7

Filtering was done for all the runs for the simulation. After filtering, the acceleration amplitude and time period were obtained, and the results have been described in the Results and Discussion section.

4. Experimental Details

In this experiment, pulse shaper(s) was mounted on a suspended heavy structure named buffer mass, and it was subjected to an impact by the striker of the test table (Fig 6 refers) with an initial velocity attained from a predefined drop height. Initially, the test table is pulled by a winch mechanism, and after getting a preset drop height, it is released, resulting in an impact on the pulse shaper. As the

striker compresses the pulse shaper during the impact, a reaction force is transmitted to the test table. During the impact process, as the velocity of the test table becomes zero, the shaper is in its maximum compressed state. Then, as a result of the reaction force, the test table again regains velocity and rebounds away from the shaper. After that, the shaper regains its original position or shape.

For the experiments, a piezoelectric accelerometer having a sensitivity of 10 mV/g was mounted on the test table near the impact point. The sampling frequency of data acquisition was 8192 Hz. With such a higher sampling frequency, there are electrical noises in the time data signal. Acquired acceleration-time data for pulse shaper thickness of 200 mm, drop height of 100, and mass of 4500 kg is shown in Fig. 8.

The noise should be eliminated from the signal to get the actual acceleration response of the structure. Therefore, the noise content in the signal is analyzed in the frequency domain with Fast Fourier Transform (FFT) analyzer. FFT of the above-shown acceleration- time data is shown in Fig 9.

FFT analysis of original data results that frequencies above 400 Hz can be eliminated from the original data. The acquired time history data was passed through a low pass filter with a cut-off frequency 400Hz to eliminate the noise in the data signal, and the result is shown in Fig.10.

Positive and negative values in acceleration - time data depend on the positioning of the accelerometer mounting and

its direction. Adequate and suitable data was acquired for varying mass, pulse shaper thickness, and drop heights. After filtering, these test results were compared with FEM results and have been reported in the Result and Discussion section.

5. Results and Discussion

This simulation obtained results for various masses, pulse shaper thickness, and impact velocities. The displacement and acceleration during impact have been observed to be a half-sine curve. A displacement graph is shown in Fig.11. Experimental values for the same impact velocities have also been recorded.

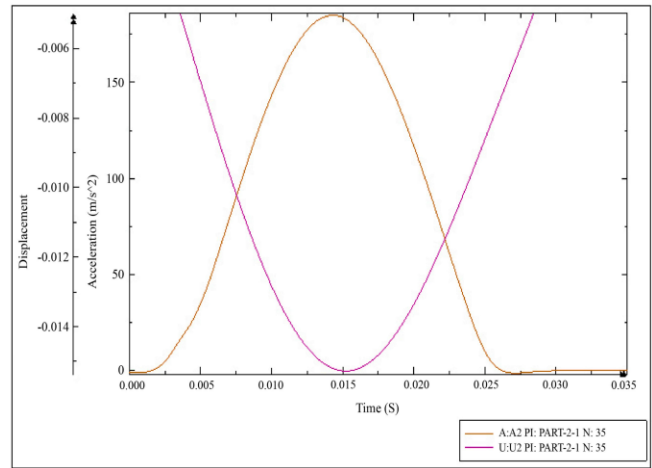


Fig. 11 Displacement graph of shaper for impact velocity 1.4 m/Sec, shaper thickness 100 mm and mass 4500 kg

Table 3. Result summary of experimental and FEM solution for mass 2100 kg

Pulse Shaper Thickness (mm)	Drop Height (mm)	Acceleration Value (g)	Time Period (ms)	Maximum Strain (%)
		% Error	% Error	
200	100	11.2	3.0	7.3
	200	9.20	4.4	9.7
	300	7.62	5.9	12.1
	400	3.4	4.7	14.1
	500	3.72	.0	15.5
	600	6.73	3.6	16.9
	700	8.08	-1.6	18.2
300	100	10.59	7.1	7.0
	200	2.52	8.0	9.3
	300	5.12	8.2	11.8
	400	6.15	8.1	13.7
	500	4.04	6.8	15.0
	600	5.02	8.3	16.4
	700	6.64	8.5	17.9
400	100	5.14	0.7	6.2
	200	4.67	-0.7	8.3
	300	5.43	1.6	10.4
	400	4.61	2.3	12.1
	500	5.33	1.2	13.3
	600	6.42	2.1	14.5
	700	7.32	1.8	15.8

Analysis was done for the acceleration response of the test object and maximum strain in the pulse shaper for each run. Acceleration response was analyzed based on acceleration amplitude and time period. FEM results were

compared with experimental results, which agreed well with the experimental results. FEM and experimental results are tabulated in Table 3, Table 4, and Table 5 for impact mass of 2100 kg, 4500 kg, and 7000 kg, respectively.

Table 4. Result summary of experimental and FEM solution for mass 4500 kg

Pulse Shaper Thickness (mm)	Drop Height (mm)	Acceleration Value(g)	Time Period(ms)	Maximum Strain (%)
		% Error	% Error	
200	100	1.1	11.1	10.8
	200	1.7	6.7	14.4
	300	2.6	7.0	17.9
	400	1.6	7.0	20.6
	500	5.0	3.5	22.6
	600	3.0	2.4	24.7
	700	2.9	2.4	26.6
300	100	1.7	13.4	10.4
	200	0.8	13.6	13.9
	300	0.9	13.8	17.4
	400	4.2	13.0	20.2
	500	5.3	12.5	22.3
	600	8.4	13.1	24.3
	700	5.6	12.3	26.3
400	100	4.2	15.6	9.2
	200	6.5	15.8	12.8
	300	1.4	17.1	15.5
	400	2.8	17.3	17.9
	500	5.3	17.1	19.7
	600	10.0	17.3	21.5
	700	9.0	17.3	23.2

Table 5. Result summary of experimental and FEM solution for mass 7000 kg

Pulse Shaper Thickness (mm)	Drop Height (mm)	Acceleration Value(g)	Time Period(ms)	Maximum Strain (%)
		% Error	% Error	
200	100	2.9	9.9	13.3
	200	6.1	7.4	17.8
	300	6.8	9.4	22.1
	400	5.2	9.4	25.9
	500	2.8	12.4	27.7
	600	5.5	11.5	30.0
	700	7.5	9.8	32.2
300	100	4.3	3.6	12.9
	200	4.5	3.8	17.3
	300	3.5	3.5	21.6
	400	1.0	3.8	25.0
	500	10.0	3.9	26.3
	600	11.1	-1.4	28.6
	700	12.0	-1.4	30.9
400	100	10.0	48.3	12.1
	200	11.9	65	16.3
	300	10.3	81.1	20.3
	400	12.5	93.8	23.5
	500	12.7	98.8	24.7
	600	12.4	107.4	26.8
	700	11.3	115.9	29

6. Effect of Drop Height and Pulse Shaper Thickness on Acceleration Amplitude

A comparative study was carried out for the effect of drop height and pulse shaper thickness on acceleration amplitude. It was concluded that acceleration amplitude increases by keeping the mass and pulse shaper thickness

constant and increasing the drop height. Similarly, keeping the mass and drop height constant and increasing the pulse shaper thickness will decrease the acceleration amplitude. Variation of acceleration with drop height and different pulse shaper thickness is shown in Fig.12, Fig.13, and Fig.14 for mass 2100 kg, 4500 kg, and 7500 kg, respectively.

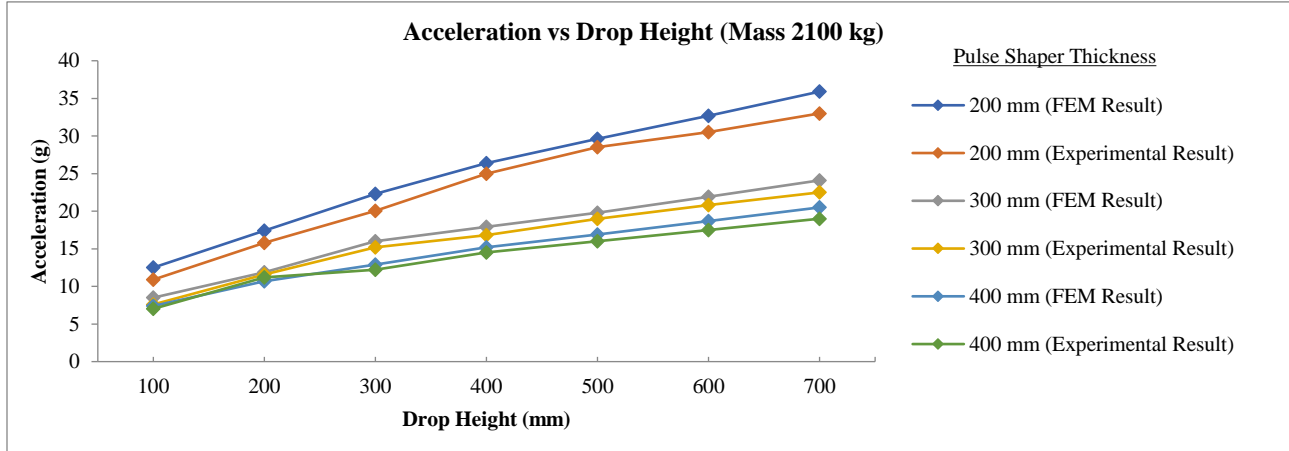


Fig. 12 Variation of acceleration with drop height and different pulse shaper thickness for mass 2100 kg

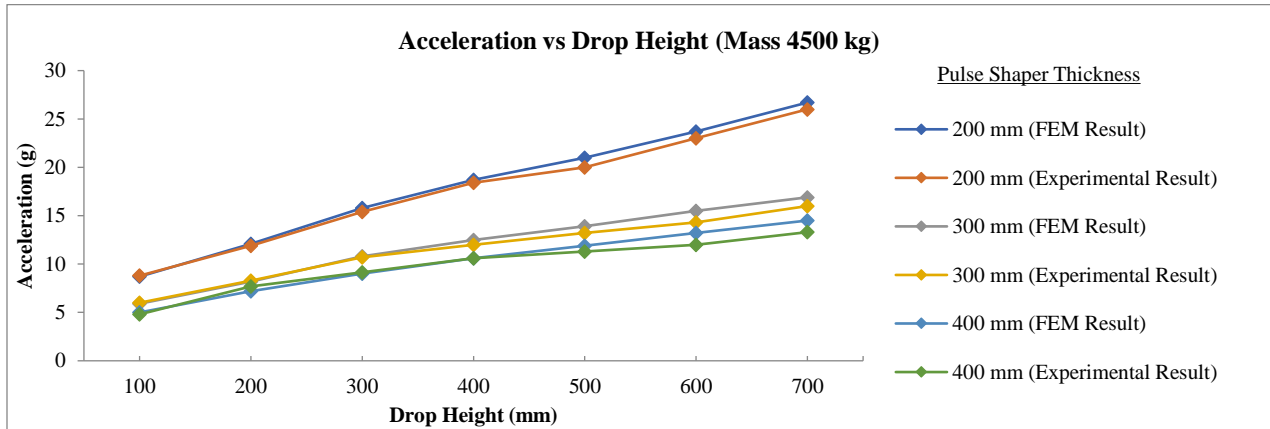


Fig. 13 Variation of acceleration with drop height and different pulse shaper thickness for mass 4500 kg

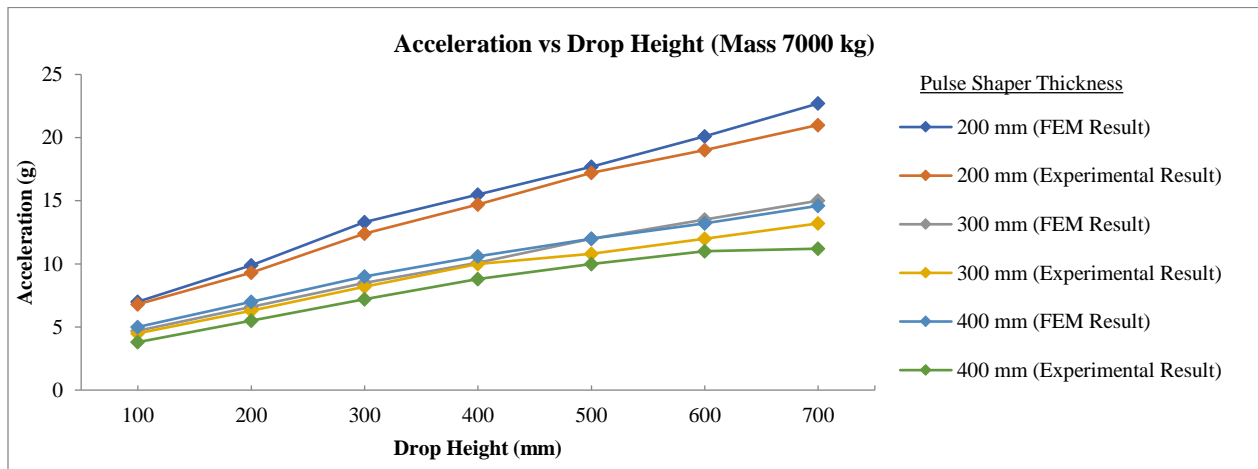


Fig. 14 Variation of acceleration with drop height and different pulse shaper thickness for mass 7000 kg

7. Effect of Drop Height And Pulse Shaper Thickness on Time Period

A subsequent study was done for the dependency of the time period on drop height and pulse shaper thickness. It was observed that the time period is not dependent on drop height

for constant mass and drop height. However, keeping the mass and drop height constant, increasing the pulse shaper thickness will increase the pulse duration. Variation of the time period with drop height and different pulse shaper thickness is shown in Fig.15, Fig.16, and Fig.17 for mass 2100 kg, 4500 kg, and 7500 kg, respectively.

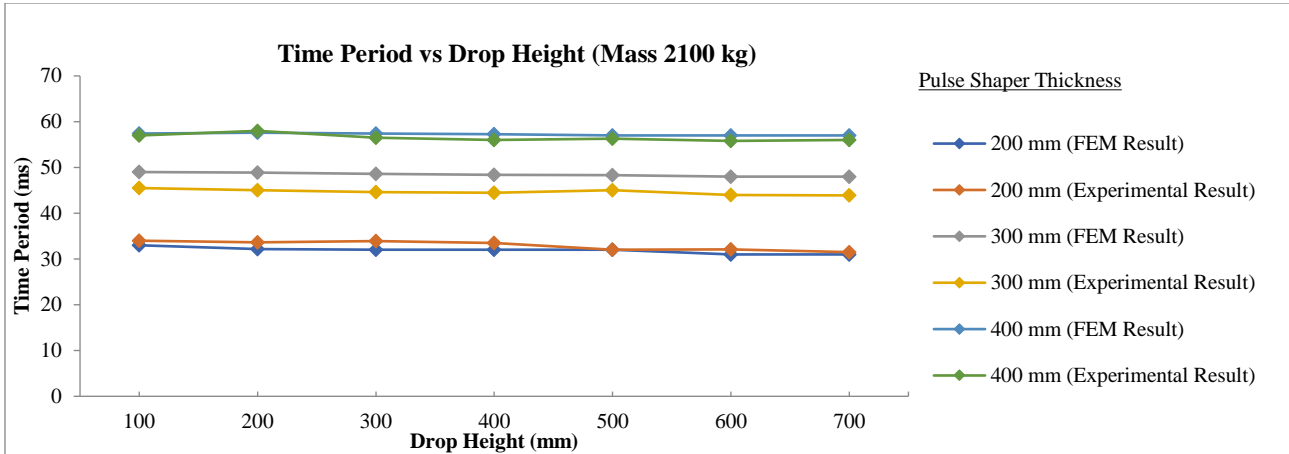


Fig. 15 Variation of the time period with drop height and different pulse shaper thickness for mass 2100 kg

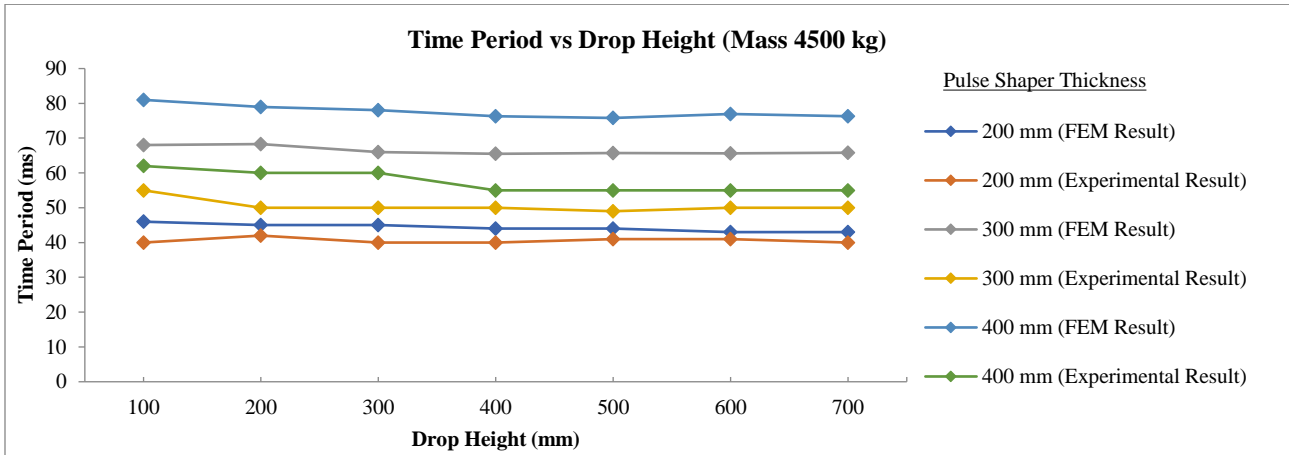


Fig. 16 Variation of the time period with drop height and different pulse shaper thickness for mass 4500 kg

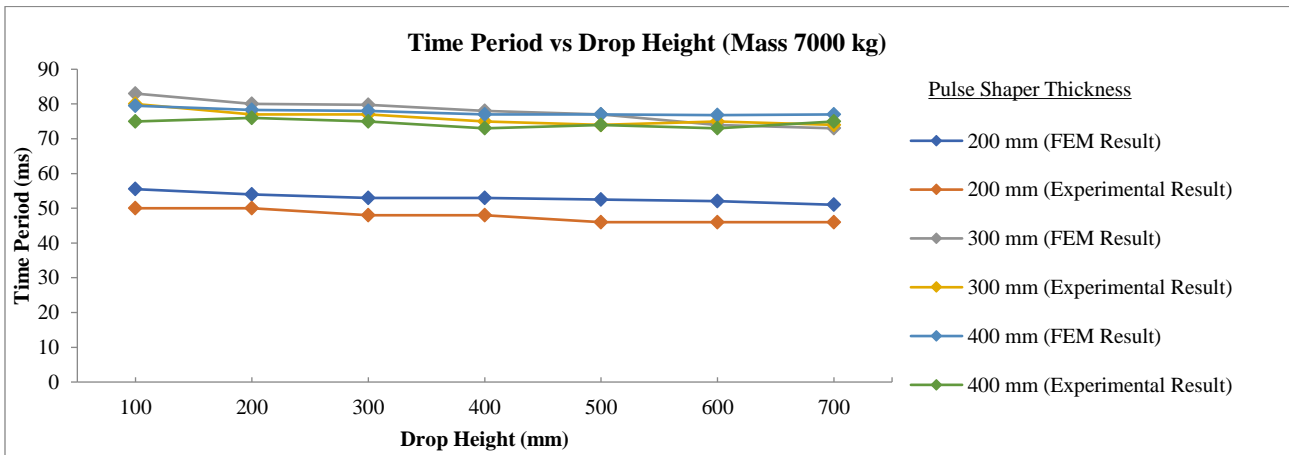


Fig. 17 Variation of the time period with drop height and different pulse shaper thickness for mass 7000 kg

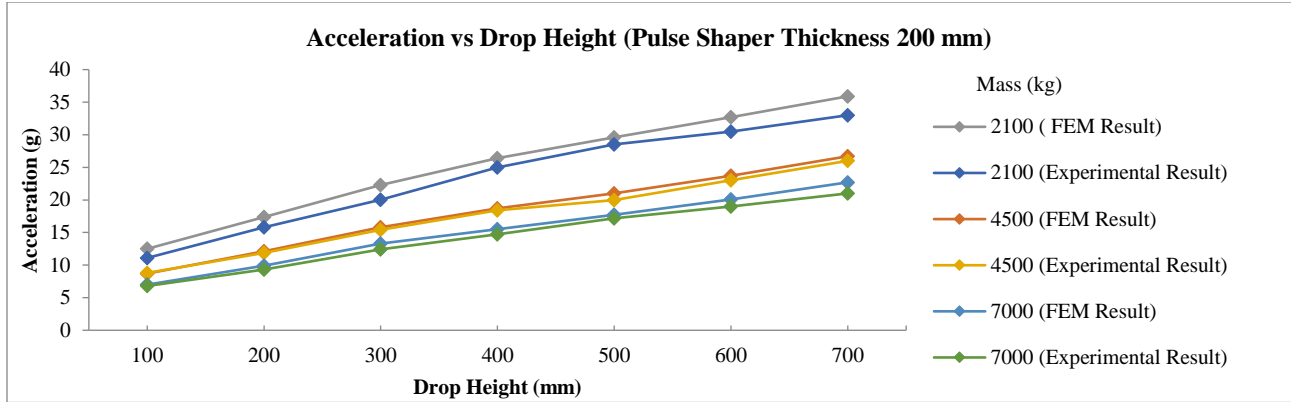


Fig. 18 Variation of acceleration with drop height and different mass

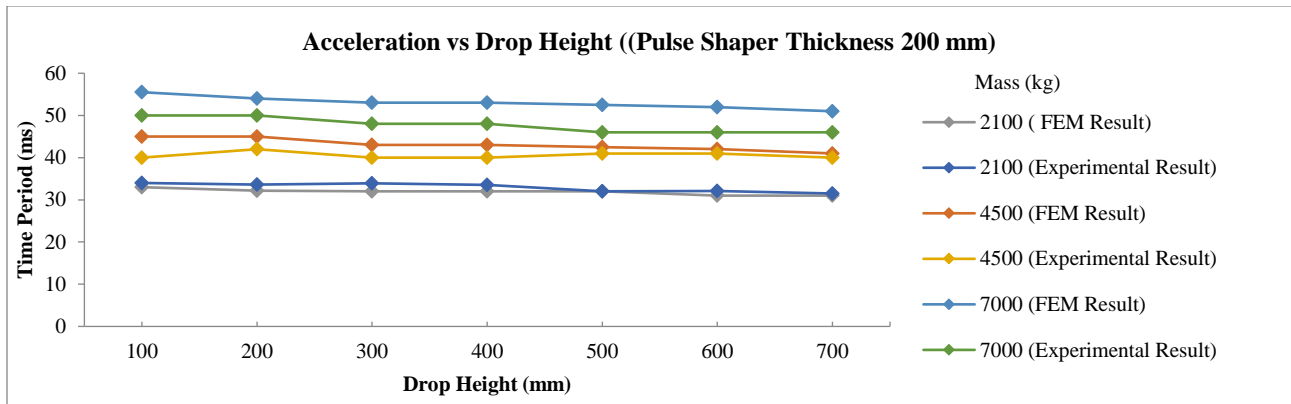


Fig. 19 Variation of the time period with drop height and different mass

8. Effect of Mass on Acceleration Amplitude and Time Period

The subsequent study was done for the effect of object mass on acceleration. It was found that keeping the pulse shaper thickness and drop height constant and increasing the object mass will decrease the acceleration amplitude on the test object. Variation of acceleration with drop height and different masses is shown in Fig.18.

FEM and experimental results were analyzed for the effect of object mass on time period. It was concluded that keeping the pulse shaper thickness and drop height constant, increasing the object mass will increase the time period of the shock pulse on the test object. Variation of the time period with drop height and different masses is shown in Fig.19.

9. Conclusion

In this study, shock pulse has been determined for three impact masses of 2100 kg, 4500 kg, and 7000 kg. The shock pulse of each mass has been varied with different pulse shaper thicknesses of 200 mm, 300 mm, and 400 mm and drop heights of 100 mm to 700 mm with an interval of 100 mm. The dependency of acceleration amplitude and time period on these variables has been shown in various graphs.

The following are the significant observations made from this study.

- The deviation in acceleration amplitude of FEM results compared with experimental results is less than 13%.
- Acceleration depends on drop height and pulse shaper thickness for a given mass.
- Increasing the drop height will increase the acceleration on the test object, and increasing the pulse shaper thickness will decrease the acceleration value.
- The time period mainly depends on pulse shaper thickness and increases with an increase in the pulse shaper thickness.
- There is no effect of drop height on the time period.
- The Acceleration decreases with an increase in the mass of the test object.
- The Time period increases with the increase in mass of the test object.
- The Maximum strain on the pulse shaper was observed as 32 %, less than the permitted strain value of 40%.

Acknowledgment

The authors would like to thank the Research and Development Establishment (Engineers), Pune, Maharashtra, India, and the Defence Institute of Advanced Technology (DU), Ministry of Defence, Pune, Maharashtra, India, for encouragement and support.

References

- [1] Harris, Cyril M. Shock and Vibration Handbook, Mcgraw-Hill, 1988. [[Google Scholar](#)] [[Publisher Link](#)]
- [2] P.F. Cunniff, and G.J. O'Hara, "A Procedure for Generating Shock Design Values," *Journal of Sound and Vibration*, vol. 134, no. 1, pp. 155-164, 1989. [[CrossRef](#)] [[Google Scholar](#)] [[Publisher Link](#)]
- [3] Naman Agrawal, Janmit Raj, and Gaurav Saxena, "Design and Analysis of Impact Attenuator: A Review," *SSRG International Journal of Mechanical Engineering*, vol. 2, no. 12, pp. 1-7, 2015. [[CrossRef](#)] [[Google Scholar](#)] [[Publisher Link](#)]
- [4] Vesta Bateman, Fred Brown, and Neil Davie, "Use of a Beryllium Hopkinson Bar to Characterize a Piezo Resistive Accelerometer in Shock Environments," *Journal of the IEST*, vol. 39, no. 6, pp. 33-39, 1996. [[CrossRef](#)] [[Google Scholar](#)] [[Publisher Link](#)]
- [5] Wei-Yang Lu et al., "Dynamic Loading of LIGA Structures," *Proceedings of SEM Annual Conference & Exposition on Experimental & Applied Mechanics*, vol. 3, pp. 1232-1239, 2006. [[Google Scholar](#)] [[Publisher Link](#)]
- [6] Yeoman, Hargrove, "Improvement of a Helmet Test Rig for Endlessly Textile Secure Riot Helmets," *SSRG International Journal of Polymer and Textile Engineering*, vol. 4, no. 3, pp. 6-10, 2017. [[CrossRef](#)] [[Publisher Link](#)]
- [7] Chao-Rong Chen et al., "Determination of Optimal Drop Height in Free-Fall Shock Test Using Regression Analysis and Back-Propagation Neural Network," *Shock and Vibration*, vol. 2014, pp. 1-10, 2014. [[CrossRef](#)] [[Google Scholar](#)] [[Publisher Link](#)]
- [8] ASTM Designation D 575, Standard Test Methods for Rubber Properties in Compression, American Society for Testing and Material, [Online]. Available: <https://file.yzimgs.com/395203/2013090611090838.pdf>
- [9] Amit Nemade et al., "Pressure and Support Analysis of an Air Receiver Using FEM," *SSRG International Journal of Mechanical Engineering*, vol. 7, no. 6, pp. 24-27, 2020. [[CrossRef](#)] [[Publisher Link](#)]
- [10] Muhammad Zahid Iqbal, and Asif Israr, "To Predict a Shock Pulse Using Non-Linear Dynamic Model of Rubber Waveform Generator," *International Journal of Impact Engineering*, vol. 147, 2021. [[CrossRef](#)] [[Google Scholar](#)] [[Publisher Link](#)]
- [11] Sagar K G, and Suresh P M, "Finite Element Analysis For Material and Geometrical Nonlinearity in Powder Compact Components," *SSRG International Journal of Mechanical Engineering*, vol. 5, no. 2, pp. 1-4, 2018. [[CrossRef](#)] [[Google Scholar](#)] [[Publisher Link](#)]
- [12] Jingjing Wen et al., "A Nonlinear Dynamic Model and Parameters Identification Method for Predicting the Shock Pulse of Rubber Waveform Generator," *International Journal of Impact Engineering*, vol. 120, pp. 1-15, 2018. [[CrossRef](#)] [[Google Scholar](#)] [[Publisher Link](#)]
- [13] Sweta Kuraria, and Veerendra Kumar, "Biomechanical Analysis of Pelvic Bone: A Review," *SSRG International Journal of Mechanical Engineering*, vol. 3, no. 7, pp. 1-4, 2016. [[CrossRef](#)] [[Publisher Link](#)]
- [14] Gongxian Wang, Yeping Xiong, and Wenzhi Tang, "A Novel Heavy-Weight Shock Test Machine for Simulating Underwater Explosive Shock Environment: Mathematical Modeling and Mechanism Analysis," *International Journal of Mechanical Sciences*, vol. 77, pp. 239-248. [[CrossRef](#)] [[Google Scholar](#)] [[Publisher Link](#)]
- [15] Edouard Diouf, and Jérémie Gaston Sambou, "Contribution of Constraints in Isotropic and Anisotropic Models," *SSRG International Journal of Mechanical Engineering*, vol. 6, no. 6, pp. 42-47, 2019. [[CrossRef](#)] [[Publisher Link](#)]
- [16] Andrés García-Pérez et al., "Overview and Application of FEA Methods for Shock Analysis in Space Instruments," *Aerospace Science and Technology*, vol. 80, pp. 572–586, 2018. [[CrossRef](#)] [[Google Scholar](#)] [[Publisher Link](#)]
- [17] Purnendu Monda, and Subramaniam Arunachalam, "Modelling the Car Seated Human Body Using Composite Ellipsoidal Bodies and Evaluation of Size and Shape Specific Stiffness Data For Various Human Segments," *SSRG International Journal of Mechanical Engineering*, vol. 7, no. 2, pp. 26-32, 2020. [[CrossRef](#)] [[Google Scholar](#)] [[Publisher Link](#)]
- [18] OMF Morais, and CMA Vasques, "Shock Environment Design for Space Equipment Testing," *Proceedings Journal of Aerospace Engineering*, vol. 231, no. 6, pp. 1154– 1167, 2016. [[CrossRef](#)] [[Google Scholar](#)] [[Publisher Link](#)]
- [19] Eter Nikitin, Ivan Smirnov, and Slava Slesarenko, "Distinct Buckling Modes in Mechanical Metamaterials with Stiff Square Networks and Periodically Arranged Voids," *International Journal of Engineering Trends and Technology*, vol. 69, no. 4, pp. 177-182, 2021. [[CrossRef](#)] [[Google Scholar](#)] [[Publisher Link](#)]
- [20] Clemens A.J. Beijers, and Andre de Boer, "Numerical Modeling of Rubber Vibration Isolators," *10th International Congress on Sound and Vibration*, pp. 805-812, 2003. [[Google Scholar](#)] [[Publisher Link](#)]
- [21] R. W. Ogden, G. Saccomandi, and I. Sgura, "Fitting Hyperelastic Models to Experimental Data," *Computational Mechanics*, p. 484-502, 2004. [[CrossRef](#)] [[Google Scholar](#)] [[Publisher Link](#)]
- [22] Alan N. Gent, *Engineering with Rubber*, Hanser Publications, Cincinnati, 3rd Edition, p. 433, 2012. [[Google Scholar](#)] [[Publisher Link](#)]
- [23] Patrick L. Walter, "Selecting Accelerometers for Mechanical Shock Measurements," *Sound and Vibration*, 2007. [[Google Scholar](#)] [[Publisher Link](#)]